

# Measurement of acoustic and anatomic changes in oral and maxillofacial surgery patients

Daniel Aalto<sup>1,2</sup>, Olli Aaltonen<sup>2</sup>, Risto-Pekka Happonen<sup>3,4</sup>,  
Päivi Jääsaari<sup>3</sup>, Atle Kivelä<sup>5</sup>, Juha Kuortti<sup>5</sup>, Jean-Marc Luukinen<sup>3,4</sup>,  
Jarmo Malinen<sup>5,\*</sup>, Tiina Murtola<sup>5</sup>, Riitta Parkkola<sup>6</sup>,  
Jani Saunavaara<sup>6</sup>, Tero Soukka<sup>3,4</sup>, Martti Vainio<sup>2</sup>

June 1, 2022

## Abstract

We describe an arrangement for simultaneous recording of speech and geometry of vocal tract in patients undergoing surgery involving this area. Experimental design is considered from an articulatory phonetic point of view. The speech and noise signals are recorded with an acoustic-electrical arrangement. The vocal tract is simultaneously imaged with MRI. A MATLAB-based system controls the timing of speech recording and MR image acquisition. The speech signals are cleaned from acoustic MRI noise by a non-linear signal processing algorithm. Finally, a vowel data set from pilot experiments is compared with validation data from anechoic chamber as well as with Helmholtz resonances of the vocal tract volume.

**Index Terms:** speech, sound recording, MRI, noise reduction, formant analysis.

## 1 Introduction

### Background

Literate people in a language are taught to think that speaking is like writing, and that a speaker produces a distinctive acoustic pattern of energy for every distinct vowel and consonant that we perceive, much as a typewriter produces letters. However, this spelling out loud is not the way we speak; spelling is a far too slow and tedious for human communication. If human speech were segmented at the acoustic level, the task of speech perception would be simply

<sup>1</sup>Dept. of Signal Processing and Acoustics, Aalto University, Finland

<sup>2</sup>Institute of Behavioural Sciences (SigMe group), University of Helsinki, Finland

<sup>3</sup>Dept. of Oral Diseases, Turku University Hospital, Finland

<sup>4</sup>Dept. Oral and Maxillofacial Surgery, University of Turku, Finland

<sup>5</sup>Dept. of Mathematics and System Analysis, Aalto University, Finland

<sup>6</sup>Dept. of Radiology, Medical Imaging Centre of Southwest Finland, University of Turku, Finland

\* Corresponding author: jarmo.malinen@aalto.fi

a matter of identifying sounds one-by-one from the speech signal, chaining them into words, and associating these with meanings stored in memory.

Speech, however, is not perceived, produced, or neurally programmed on a segmental basis. Instead, utterances are produced and perceived as a whole. It should be emphasised that we perceive speech by virtue of our tacit knowledge of how speech is produced. Thus, the elements of speech are *articulatory gestures*, not the sounds these phonetic gestures produce. The gestures are the ultimate constituents of language which must be exchanged between a speaker and a listener if communication through language is to occur.

The human articulatory system is the only one anatomically and neurally efficient enough to produce acrobatic manouvers of speech organs fast, without errors, and with minimal energy. The main vocal tract elements used in producing phonetic gestures are the lips, tongue tip and tongue dorsum, soft palate, and the larynx. By combining their movements in various ways meaningful linguistic units can be built up and conveyed via sound. Observing as well as modelling the related biophysical features and dynamic phenomena is far from a trivial matter even if state-of-the-art instruments and methods (such as computational modelling based on modern medical imaging technologies) are available. Challenging as they are, these approaches appear quite promising for adding to our current understanding of what happens during normal or pathological speech.

### **Modelling based on multi-modal data sets**

Perhaps the most important reason for using modelling and simulations is the inherent difficulty in observing speech biophysics in test subjects directly.

Mathematical models of human speech production have been used for speech analysis, processing, and synthesis as well as studying speech production acoustics for a long time; see, e.g., [9, 14, 16]. Many of the earlier numerical models were based on radical simplifications of the underlying physics and anatomic geometry, such as the Kelly–Lochbaum model [19] and many approaches of transmission line type; see, e.g., [11, 12, 25]. Due to modern fast and cheap computing of large scale systems, heavier numerical acoustics models [15, 20, 35, 40] and computational flow mechanics models [17, 38] have replaced earlier approaches where higher resolution is required.

This article has been written having in mind the wave equation (or its resonance version, the Helmholtz equation) and Webster’s horn model for simulating the vocal tract acoustics. These models are well-suited for studying speech acoustics for medical purposes as well as for basic research in speech sciences, and it depends crucially on getting high resolution geometries of the whole speech apparatus. It is further expected that incorporating soft tissue and muscles into such models, their usability would ultimately extend into studying normal and pathological speech production from an articulatory point of view [10, 27, 39]. This provides novel and efficient tools for planning and evaluating oral and maxillofacial surgery and rehabilitation; see, e.g., [26, 36] for background.

Before a numerical model for speech production (such as discussed in, e.g., [1, 2, 3, 15]) can be used for any practical or theoretical purpose, there are always some model parameters that need to be estimated based on measurements from human subjects. Such parameters, of course, include the geometry of the vocal

and the nasal tracts from the lips and nostrils to the beginning of the trachea. To have sufficient degree of confidence in the simulation results, any such model must have been rigorously validated by extensively and methodically comparing simulated speech sounds (or their characteristics) to measurements. One way of doing the validation is by comparing the measured and the simulated formants (related to the acoustic resonances of the vocal tract) as has been done in [6] using a Helmholtz resonance model. In any case, the validation of the computational model depends on recording a coupled data set: speech sound and the precise anatomy which produces it. We emphasize that such a multi-modal data set is quite interesting for other reasons that have little to do with mathematical and numerical modelling [29].

### **Purpose and outline of the article**

We have developed an experimental arrangement to collect a multi-modal data set using simultaneous Magnetic Resonance Imaging (MRI) and speech recordings as reported in [21, 24]. The experimental arrangement includes custom hardware, software, and experimental protocols. During a pilot stage in June 2010, a set of measurements were carried out on a healthy 30-year-old male subject, confirming the feasibility of the arrangement and the high quality of the data obtained [4, 30]. These pilot measurements also revealed a number of issues to be addressed before tackling the main objective: obtaining a clinically relevant data set from a large number of patients.

The purpose of this article is to describe the final experimental arrangement including the improvements which take into account these issues. A second pilot experiment was carried out in June 2012 on a healthy 26-year-old male subject in order to validate the final experimental setup. The geometric data in Fig. 3 as well as the spectral envelopes of recorded vowel signals in Figs. 6–7 are from these experiments. All patient data is excluded from this article.

This article consists of three parts that document the main aspects of MRI experiments during speech. In Section 2 the experimental design is discussed from the phonetic and physiologic points of view. Technical questions related to MRI and the simultaneous speech recording are discussed in Section 3. The acoustic instrumentation is treated only briefly, and we refer to earlier work [4, 21, 24, 30] for details. Instead, we concentrate on the software and digital parts of the measurement system, optimisation of the MRI sequences, and the automated control and timing of the experiments. The last part of this article, Section 4, is devoted to digital signal processing of the recorded signals: removing acoustic MRI noise and artefacts, extracting formants, and validating results.

### **Selection of the patient groups**

We describe experimental procedures that have been designed to assess acoustic and anatomic changes in patients undergoing oral or maxillofacial surgery which causes changes in the vocal tract. Patients of orthognatic surgery are a particularly attractive study group for mathematical modelling of the speech production. Not only are these patients mostly young adults without any significant underlying diseases, but there is a strong medical motivation for a comparative study of their pre- and post-operative speech as well.

Orthognatic surgery deals with the correction of abnormalities of the facial tissues. The underlying cause for abnormality may be present at birth or may be acquired during the life as the result of distorted growth. Orthodontic treatment alone is not adequate in many cases due to severity of the deformities. In a typical operation, the position of either one jaw (mandible or maxilla) or both jaws is surgically changed in relation to the skull base. The movement of the jaw position varies usually between 5–15 mm either to anterior or posterior direction. Such a considerable movement has a profound effect on the shape and volume of vocal tract, resulting detectable changes in acoustics [26]. Although the surgery involves mandibular and maxillary bone, changes occur also in the position and shape of the soft tissues defining the vocal tract. Such change is easily quantifiable using MRI.

At the time of writing of this article, seven patients of orthognatic surgery (out of which four are female) have undergone their pre-operative MRI examinations following the methods and protocols described here. We expect to enroll the total of 20 patients (10 adults of both sexes) in this research.

## 2 Experimental arrangement

Generally speaking, the experimental setting is similar to the setting in which the pilot arrangement was tested [4, 30] but with numerous improvements. They are related to instructing and cueing the patient, the role of the experimenter, and the automated control and timing of MR imaging.

The creation of the original pilot data reported in [4] required 3 – 4 people working simultaneously in the MRI control room. The improved arrangement described in this article requires only two people: one for MR imaging and the other for running the integrated experimental control system and sound recording. Moreover, it is now possible to produce over 60 takes during a session of 1 h which is about three times as fast data a collection rate as can be attained using a non-automated system. The streamlining of all procedures is vital because laboratory downtime and cost must be minimised when gathering a large data set. Also patient comfort and performance are compromised by overly long MRI sessions.

### 2.1 Phonetic material

The speech materials have been chosen to provide a phonetically rich data set of Finnish speech sounds. The chosen MRI sequences require up to 11.6 s of continuous articulation in a stationary position. We use the Finnish speech sounds for which this is possible: vowels [a, e, i, o, u, y, æ, œ], nasals [m, n], and the approximant [l]. A long phonation is possible also for, e.g., [j, s, ʃ] but these have been excluded because of unpleasantness in supine production ([ŋ]) and turbulences in the vocal tract ([j, s]).

Patients are instructed to produce each of the sounds at a sustained fundamental frequency ( $f_0$ ). We use two different  $f_0$  levels (104 and 130 Hz for men, 168 and 210 Hz for women) for the sounds [a] and [i] to obtain the vocal tract geometry with different larynx positions. The rest of the sounds are produced at the lower  $f_0$  only. The  $f_0$  levels have been matched with the acoustic MRI noise frequency profile to avoid interference.

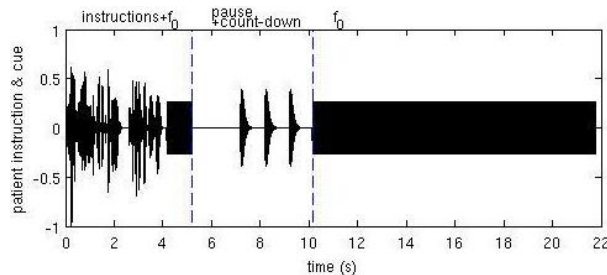


Figure 1: *Patient instruction and cue signal structure.*

In a sustained phonation, the long exhalation causes contraction in the thorax and hence a change in the shape of vocal organs. The stationary 3D imaging sequence which is used to obtain the vocal tract geometry provides no information on this adaptation process, so additional dynamic 2D imaging on the mid-sagittal section for the sounds [a, i, u, n, l] is used to monitor articulatory stability.

Speech context data is also acquired by having the patient repeat 12 sentences which have been selected from a phonetically balanced sentence set [37]. A few syllable repetition measurements (“tattatta”, “kikkikki”, etc.) are done, too. These continuous speech samples are imaged using the same dynamic 2D sequence which is used for checking articulatory stability.

An instruction and cue signal is used to guide the patient through each measurement. The signal consists of three parts as shown in Fig. 1: (i) recorded instructions specifying the task with a sample of the desired  $f_0$ , (ii) a 2 s pause and three count-down beeps one second apart, and (iii) continuous  $f_0$  for 11.6 s. In case of speech context experiments, the recorded instructions specify the sentence to be repeated and  $f_0$  is left empty in both parts (i) and (iii). Audibility of the  $f_0$  cues over MR imaging noise is achieved by using a sawtooth waveform.

## 2.2 Setting for experiments

The patient lies supine inside the MRI machine with a sound collector placed on the Head Coil in front of the patient’s mouth. The patient can communicate with the control room through the sound collector and the earphones of the MRI machine. The patient can also hear his own (de-noised) voice through the headphones with a delay of approximately 90 ms.

The patients familiarise themselves with the tasks and the phonetic materials before the beginning of a measurement session. They also practice the tasks under the supervision and are given feedback on their performance. At the start of a measurement, the experimenter selects the phonetic task. The patient then hears the recorded instructions. The instructions and the following pause and count-down beeps give the patient time to swallow, exhale, and inhale before phonation is started after the count-down beeps. The patient hears the target  $f_0$  in the earphones added to his own (de-noised) voice throughout the phonation.

MR imaging for static 3D and dynamic stability check sequences is started 2 s after the start of phonation and finishes approximately 500 ms before the end of phonation. Thus “pure samples” of stabilised utterance are available before and after the imaging sequence. Two 200 ms breaks are inserted into

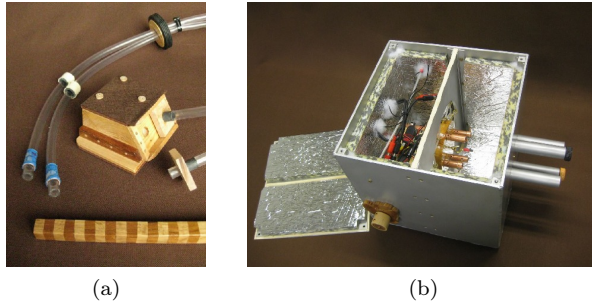


Figure 2: (a) The sound collector with one of the two audio wave guides attached. (b) The microphone array inside the Faraday cage.

the MRI sequences. The duration of these breaks has been determined based on the half-time of the imaging noise in the MRI room, which was measured to be approximately 20 ms. Sentence and syllable imaging sequences start simultaneously with phonation and end after 3.2 s.

The experimenter listens to the speech sound throughout the experiment, allowing unsuccessful utterances to be detected immediately. At the end of the experiment, the experimenter writes comments and observations into a metadata file. The recorded sound pressure levels are also inspected. Unsuccessful measurements are repeated, at the experimenter’s discretion, either immediately or later in the measurement set.

### 3 Simultaneous MRI and speech recording

The MRI room presents a challenging environment for sound recording due to acoustic noise and interference to electronics from the MRI machine. For safety and image quality reasons, use of metal is restricted inside the MRI room and prohibited near the MRI machine. Our approach is to use passive acoustic instruments for collecting the sound samples and transmitting them to a safe distance from the MRI machine. Alternative solutions are (i) using an optical microphone inside the MRI machine [28], (ii) recording by conventional directional microphones sufficiently far away from the MRI machine that has an open construction [32, 33], and (iii) using the internal microphone of the MRI machine [39].

#### 3.1 Speech recording

We use instrumentation specially developed for speech recording during MRI [21, 24]: A two-channel sound collector (Fig. 2a) samples the speech and primary noise signals in a dipole configuration. The sound signals are coupled to a microphone array inside a sound-proof Faraday cage (Fig. 2b) by acoustic waveguides of length 3.00 m (the ends of which can be seen in Fig. 2a). Two additional “ambient noise” samples are collected: one from the microphone array inside the Faraday cage and another from inside the MRI room using a directional electret microphone near the patient’s feet, pointing towards the patient’s

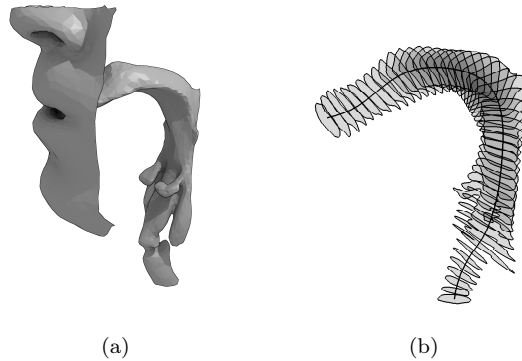


Figure 3: (a) The surface model of the tissue-air interface of a male vocal tract while pronouncing [œ]. (b) The centreline and intersection areas extracted from the same geometry.

head and the MRI coil.

The four signals are coupled from the microphones to a custom RF-proof amplifier that is situated in the measurement server rack (shown in Fig. 4a) outside the MRI room. The amplifier contains additional circuitry (i.e., a long-tailed pair with a constant emitter current source) for optimal, real time analogue subtraction of the primary noise channel from the speech channel. This is intended to produce the de-noised signal played back to the patient, and it is used for audio signal quality observation in the MRI control room as well. The final, high-quality de-noised signal is not produced this way but from digitised component signals by the algorithm discussed in Section 4. We remark that the hardware appears to be able to transmit good signal at least up to 10 kHz but we use only the phonetically relevant frequency range below 4.5 kHz where the measured frequency response is given in Fig. 4b.

Audio signals are converted between analogue and digital forms using a M-Audio Delta 1010 PCI Audio Interface. A measurement server is used which has an Intel Core i7-860 processor clocked at 2.80GHz, and is equipped with 4Gb RAM and a SSD drive for fast booting. For immediate internal data backup, three additional 1.5TB discs are set up in RAID1 configuration by a HighPoint RocketRaid 2302 controller. The whole setup is powered by an APC Smart-UPS SC 450VA, and it is installed to a portable 10U rack as shown in Fig. 4a. All user access to the server is done with laptops (in fact, MacBooks) running X11 servers, either via 1GB LAN or a wireless access point.

### 3.2 Magnetic resonance imaging

Measurements are performed on a Siemens Magnetom Avanto 1.5T scanner (Siemens Medical Solutions, Erlangen, Germany). Maximum gradient field strength of the system is 33 mT/m (x,y,z directions) and the maximum slew rate is 125 T/m/s. A 12-element Head Matrix Coil and a 4-element Neck Matrix Coil are used to cover the anatomy of interest. The coil configuration allows the use of Generalized Auto-calibrating Partially Parallel Acquisition (GRAPPA)

	3D static	2D stability	2D sentence/syllable
Pulse separation	240 ms	140 ms	150 ms
Number of slices	35	69	20
Pause after slice	12 and 24	23 and 43	no pause

Table 1: External triggering parameters used in MRI scans.

technique to accelerate acquisition. This technique is applied in all the scans using acceleration factor 2.

3D VIBE (Volumetric Interpolated Breath-hold Examination) MRI sequence [34] is used as it allows for the rapid static 3D acquisition required for the experiments. Sequence parameters have been optimized in order to minimize the acquisition time. The following parameters allow imaging with 1.8 mm isotropic voxels in 7.8 s: Time of repetition (TR) is 3.63 ms, echo time (TE) 1.19 ms, flip angle (FA)  $6^\circ$ , receiver bandwidth (BW) 600 Hz/pixel, FOV 230 mm, matrix 128x128, number of slices 44 and the slab thickness of 79.2 mm.

Dynamic MRI scans are performed using segmented ultrafast spoiled gradient echo sequence (TurboFLASH) where TR and TE have been minimized. Single sagittal plane is imaged using parameters TR 178 ms, TE 1.4 ms, FA  $6^\circ$ , BW 651 Hz/pixel, FOV 230 mm, matrix 120x160, and slice thickness 10 mm.

Siemens Magnetom Avanto 1.5T units have inputs that accept external synchronisation signals for timing the MRI sequences. We use external triggering in all three different types of experiments, and the triggering signal is always a train of 12 ms TTL level 1 pulses separated by TTL level 0 of variable duration. The pulse train is generated with a custom-made device which converts 1 kHz analogue sine signal from the sound system to the logic pulses. The details of triggering are given in Table 1.

External triggering with the additional pauses increases the 3D imaging time to 9.1 s. Post-processing of the MR images and the resolution of the obtained vocal tract geometries are discussed in [5, 6, 7].

### Visibility of teeth

Teeth are not visible in MRI but they are an important acoustic element of the vocal tract. Hence, it is necessary to add teeth geometry into the soft tissue geometry obtained from the MR images during post-processing. Optical scans of teeth or digitalised dental casts can be readily obtained from the patients but the alignment of the two geometries is a non-trivial problem. Markers containing vegetable oil, attached to the surface of the teeth, appear to be a practical approach that produces sufficient MRI visibility; see also [13]. Further work is still required to get a solution for alignment that does not require extensive manual work.

### 3.3 Control of measurements

Measurements are controlled with a custom code in MATLAB 7.11.0.584 (R2010b) running on the portable server with operating system Ubuntu 10.04 LTS on Linux 2.6.32.38 kernel (Fig. 4a). Access from MATLAB to the Audio Interface is arranged through Playrec (a MATLAB utility, [18]), QjackCtl JACK

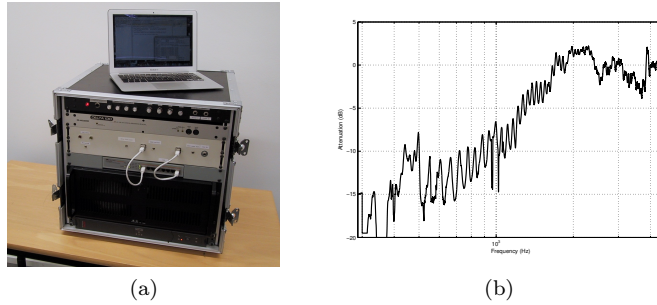


Figure 4: (a) The measurement server with the RF-proof four-channel amplifier, M-Audio Delta 1010 Audio Interface, and networking facilities. The laptop is used for remote access. (b) The measured frequency response of the whole audio signal path from the sound collector to the amplifier input. The non-flat frequency response is compensated by DSP in post-processing stage.

Audio Connection Kit (v. 0.3.4), and JackEQ 0.4.1.

The custom code computes the input signal to the MRI triggering device, reads the patient instruction and cue audio file, and assembles the two signals into a playback matrix. Recording is started simultaneously with playback and carried on for equal number of samples. In addition to the speech and the three noise signals, recording also includes the analogically de-noised signal and the patient instruction signal.

The audio configuration causes delays in the signals. MRI noise is recorded with a delay of approximately 60 ms (MRI machine delays excluded) relative to the onset of recording. This is accounted for by the method of locating the “pure samples”. Patient speech is recorded with a delay of approximately 90 ms (patient reaction time excluded), and patients also hear their own voices with this same delay. These patient speech delays may have two effects. First, the duration of the last pure sample is reduced from 500 ms to 410 ms, which makes no significant difference from the point of view of data analysis. And second, the echo effect may disturb the patient during sentence repetition in which case the speech feedback may be turned off or its volume reduced independent of the cue signal.

The control code automatically saves the recorded sounds as a six-channel Waveform Audio File. A separate file containing metadata is also saved automatically. The metadata file contains all experimental parameters, including task specification, and the locations of the pure samples in the sound file.

The control system requires user input for three tasks. First, the experimenter selects the next phonetic task (target sound or sentence and  $f_0$ ) and MR imaging sequence. Second, comments and observations may, if necessary, be written about each measurement separately. They are saved automatically in the metadata file in JSON format. And third, patient headphone volume and recorded sound pressure levels may be adjusted manually based on feedback from the patient and rudimentary post-experimental sound data checks. The sound data checks consist of histograms of recorded signal levels, and they are displayed to the experimenter automatically at the end of each measurement. This allows detection and correction of settings for which the recorded signal

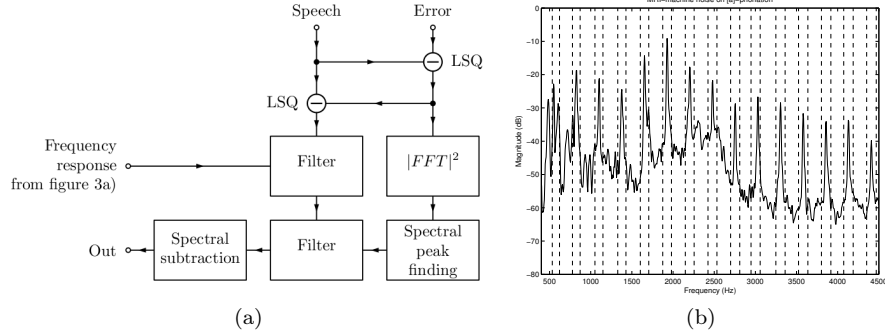


Figure 5: (a) Block diagram of the noise reduction algorithm. (b) The detected spectral noise peaks. Note the regular harmonic structure.

levels, which vary for different speech sounds, are outside the optimal range.

A single measurement takes on average 30-40 s, including task selection by the experimenter and writing additional information and observations in the metadata file. At the time of writing of this article, seven patients of orthognatic surgery have taken part in the experiments, and the times spent inside the MRI machine were between 50–95 min. When running the experiment at a comfortable pace for the patient, between 93 and 107 MRI scans were produced in a single session.

## 4 Post-processing of speech signals

### 4.1 Adaptive noise reduction

As explained in Section 3.1, two sound channels are acoustically transmitted from near the test subject inside the MRI machine. One of the channels provides the speech sample  $s(t)$  (which is contaminated by acoustic MRI noise), and the other is reserved for the acoustic MRI noise sample  $n(t)$  (which, in turn, is contaminated by speech). The analogically produced weighted difference of these signals is fed back to subject’s earphones during the experiment in almost real time. Both the signals  $s(t)$  and  $n(t)$  are also recorded separately, so that more refined numerical post-processing can be performed later.

Because of the multi-path propagation of the noise in particular around the MRI coil surfaces, the recorded noise sample is a weighted sum of more simple signals with distributed delays. As a further complication, the chassis of the MRI machine acts as a spatially disributed acoustic source, and its dimensions are large compared to wavelengths in air at frequencies of interest. Hence, some residual higher frequency noise will remain after an optimised subtraction of the noise  $n(t)$  from the contaminated speech signal  $s(t)$ . To reduce this residual noise, *adaptive spectral filtering* is used. The approach is based on the observation that the typical noise spectrum of a MRI machine consists of narrow and high peaks with significant harmonic overtones. Adaptivity is desirable because the peak positions depend on the MRI sequence used, and they are not invariant of time even within a single MRI sequence.

The noise reduction algorithm is outlined in Fig. 5a, and it consists of the following Steps 1–7 that have been realised as MATLAB code:

1. **LSQ:** Linear, least squares optimal subtraction of the noise from speech as detailed below. This reproduces roughly the same quality of speech signal that was produced analogically during the experiment for patient’s earphones in real time.
2. **Frequency response compensation:** Compensation for the measured non-flat frequency response of the measurement system, shown in Fig. 4b.
3. **Noise peak detection:** The noise power spectrum is computed by FFT, and the most prominent spectral peaks of noise are detected.
4. **Harmonic structure completion:** The set of noise peaks is completed by its expected harmonic structure to ensure that most of the noise peaks have been found; see Fig. 5b.
5. **Chebyshev peak filtering:** Each of the noise peaks defines a centre frequency of a corresponding stop band. The width of the stop band is a function of the centre frequency given by Eq. (2). The corresponding frequencies are attenuated from the de-noised speech signal (that has been produced in Step 2 above) by Chebyshev filters of order 20 at these stop bands.
6. **Low pass filtering:** The resulting signal is low pass filtered by a Chebyshev filter of order 20 and cut-off frequency 10 kHz.
7. **Spectral subtraction:** A sample of the acoustic background of the MRI room (without patient speech and the noise during the MRI sequence) is extracted from the beginning of the speech recording. Finally, the averaged spectrum of this is subtracted from the speech signal in frequency plane using FFT and inverse FFT; see [8].

The optimal linear subtraction in Step 1 is carried out by producing de-noised signals  $\tilde{s}(t)$ ,  $\tilde{n}(t)$  from the original signals  $s(t)$  and  $n(t)$  according to

$$\tilde{n} = n - \frac{\langle n, s \rangle}{\|n\| \cdot \|s\|} s \quad \text{and} \quad \tilde{s} = s - \frac{\langle s, \tilde{n} \rangle}{\|s\| \cdot \|\tilde{n}\|} \tilde{n} \quad (1)$$

where  $\langle n, s \rangle = \int n(t)s(t) dt$  and  $\|s\|^2 = \langle s, s \rangle$ . The bandwidths in Step 5 are given as a function of the centre frequency  $f$  by

$$w(f) = C \ln f \quad \text{where} \quad w(550 \text{ Hz}) = 50 \text{ Hz}. \quad (2)$$

The numerical parameters values (i.e., the bandwidth parameter  $C$ , the filter order, and the cut-off frequency) have been determined by trial and error to get audibly good separation of speech and noise in prolonged vowel samples. In particular, choosing the bandwidth parameter  $C$  for Step 5 is crucial for the outcome. The cut-off frequency of 10 kHz in Step 6 is chosen well above the phonetically relevant part of the frequency range that extends upto 4.5 kHz corresponding to Fig. 4b.

The algorithm produces de-noised speech signals where the S/N ratio is audibly much improved compared to the mere optimal subtraction as defined in

Eq. (1). Each speech sample contains 2 s of undisturbed speech before acoustic MRI noise starts, and comparing the amplitude of the speech channel signal just before and right after the noise onset, we can get an estimate for the S/N ratio (assuming that the speech amplitude remains reasonably constant at the MRI noise onset, and that speech and noise are uncorrelated). Moreover, the S/N ratio depends on the vowel because the emitted acoustic power tends to be larger for vowels with larger mouth opening area. As a rule of thumb, we obtain cleaned-up vowel signals whose S/N ratio lies between 1.9 dB and 3.6 dB, the average being 2.8 dB. The Chebyshev filtering in Step 5 creates a somewhat “robotic” tone to speech signals but we have not carried out perceptual evaluation of the de-noised signals as was done in [29].

The subtraction of noise with a “spiky” power spectrum from, e.g., speech is a classical problem in audio signal processing. The non-linear *cepstral transform* is a popular procedure, and it has been used successfully in [32] for MRI noise cancellation. This algorithm is based on computing the logarithm of the power spectrum (in order to compress all high spectral peaks “softly” and non-adaptively), returning to time domain by FFT, and reconstructing the phase information from the original signal. The cepstral transform does not take into account the harmonic structure of noise at all. The multi-path propagation of noise would seem to invite an approach based on *deconvolution*. However, an accurate estimation of the convolution kernel (i.e., the delays and the weights in multi-path propagation) does not seem to be feasible even though the auto-correlation of the noise signal is easy to compute.

## 4.2 Extracting power spectra and spectral envelopes

Formants are the main information bearing component of vowel sounds. They can be understood as acoustic energy concentrations around discrete frequencies in the power spectrum of the speech signal. The measured formant frequencies  $F_1, F_2, \dots$  are related to the acoustic resonance frequencies  $R_1, R_2, \dots$  of the vocal tract. In contrast to harmonic overtones of the fundamental frequency  $f_0$  of the glottal excitation, the formants have a much wider bandwidth. Thus, the extraction of formants from speech can be carried out by a frequency domain smoothing process that downplays the narrow bandwidth harmonics of  $f_0$ .

Perhaps the most popular formant extraction tool is Linear Predictive Coding (LPC); see, e.g., [22, 23]. LPC is mathematically equivalent to fitting a low-order rational function  $R(s)$  to the power spectrum function defined on the imaginary axis, and the pole positions of  $R(s)$  give the estimated formant values. Hence, plotting the values of  $|R(i\omega)|$  for real  $\omega$  yields *LPC envelopes* whose peaks indicate the formant frequencies  $F_1, F_2, \dots$

A number of LPC envelopes, produced by the MATLAB function `lpc`, for each the eight Finnish vowel [a, e, i, o, u, y, æ, ø] are given in Figs. 6–7. All the data has been recorded from a healthy 26-year-old male in supine position. There are samples during an MRI scan as well as comparison samples that have been recorded in an anechoic chamber. Three lowest acoustic resonances have been computed by FEM, based on the vocal tract geometries obtained by MRI.

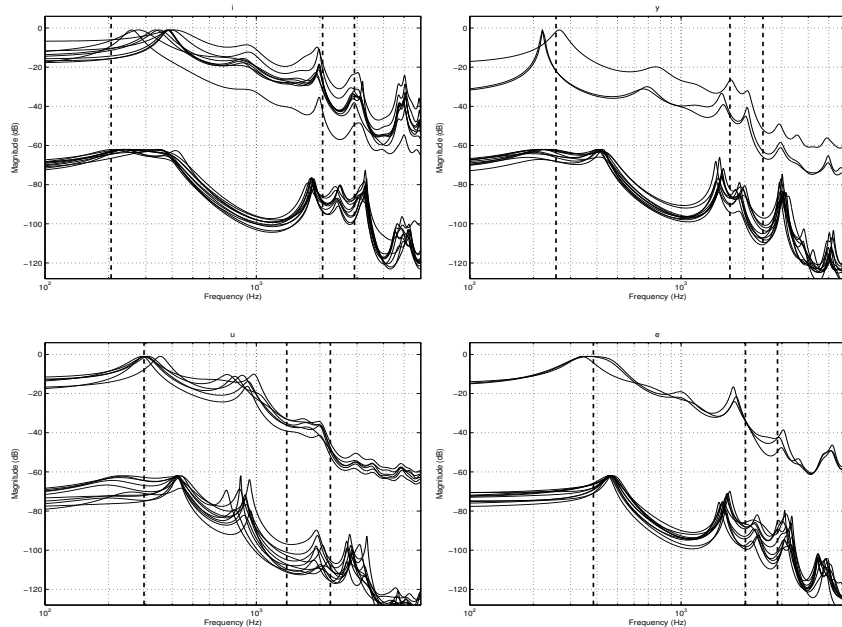


Figure 6: Spaghetti plots of LPC envelopes from Finnish front vowels [i, y, u, e] in the order of increasing  $F_1$ . In each panel, the upper graphs have been produced from recordings during the MRI using the noise reduction detailed in Section 4.1. The lower graphs have been produced from recordings in anechoic chamber from the same test subject. The vertical dotted lines are the three lowest resonance frequencies  $R_1, R_2$ , and  $R_3$ , computed by FEM from one of the MRI geometries using the Helmholtz model in [15].

### Sound data during MRI

As pointed out in Section 1, a second set of pilot MRI experiments was carried out in 2012. The test subject was able to produce 107 speech samples during a single MRI session of 1.5 h according to the experimental specifications given in Section 2. Out of these speech and MRI samples, 69 are vowels imaged by static 3D MRI, out of which 40 with  $f_0 \approx 104$  Hz were chosen for the validation experiment.

The vowel samples were processed by the noise reduction algorithm detailed in Section 4.1, and their LPC envelopes (using filter order 40) shown in Figs. 6–7 were produced by MATLAB. In many but not in all cases, the lowest formants  $F_1, F_2$ , and  $F_3$  could be correctly revealed by Praat [31] (using default settings) from the de-noised signals.

### Comparison sound data from anechoic chamber

To obtain high-quality comparison data, speech samples were recorded in anechoic chamber from the same subject in supine position. Brüel & Kjæll 2238 Mediator integrating sound level meter was used as a microphone, coupled to RME Babyface digitizer with software TotalMix FX v.0.989 and Audacity v.1.3.14 running on MacBook Air OSX 10.7.5. The test subject heard from earphones

his own, algorithmically de-noised speech signal from pilot MRI experiments as a pitch reference. The vowels were given in a randomised order and also shown on a computer screen.

Even though these experiments were designed to resemble the conditions during the MRI scan in many respects, there are significant differences. Firstly, the acoustic noise of the MRI machine was not replicated in the anechoic chamber. Secondly, the test subject fatigue played lesser role in anechoic chamber since the total duration of a single experimental session was only about 10 minutes. Thirdly, the head and neck MRI coil is a rather closed acoustic environment whereas there was no similar acoustic load present in the anechoic chamber. Reflections from the MRI coil walls produce spurious “external formants” to measured speech signals, and we believe this to be the explanation for some of the extra peaks that can be seen the upper curves in Figs. 6–7.

### Computation of the Helmholtz resonances

For each vowel presented in Figs. 6–7, one MRI scan was randomly chosen from the full set. This MRI geometry was processed as described in [5] to produce surface models of the air-tissue interface as shown in Fig. 3. The models did not include teeth geometries at all.

The FEM mesh was generated from the surface model, and the acoustic resonances  $R_1, R_2 \dots$ , of the vocal tract air column were computed using the Helmholtz resonance model detailed in [15]. The Dirichlet boundary condition (which is a very rudimentary exterior space acoustic model indeed) was used at the mouth, leading to an overestimation of  $F_2$  and  $F_3$  by the respective  $R_2$  and  $R_3$ . The FEM computation reveals a cloud of higher Helmholtz resonances  $R_4, R_5, R_6, \dots$  near the expected fourth formant  $F_4$  position (as given by Praat v.4.6.15 or `lpc` in MATLAB) but they are not shown in Figs. 6–7.

## 5 Conclusions

We have described experimental protocols, MRI sequences, a sound recording system, and a customised post-processing algorithm for contaminated speech that, in conjunction with previously reported arrangements [4, 21, 24, 30], can be used for simultaneous speech sound and anatomical data acquisition on a large number of oral and maxillofacial surgery patients.

The data set obtained from these measurements are primarily intended for parameter estimation, fine tuning, and validation of a mathematical model for speech production. However, these methods and procedures may be used in a wider range of applications, including medical research and clinical use.

Collecting such multi-modal data from a large set of patients is far from a trivial task even when suitable instrumentation is available. Several phonetic aspects must be taken into account to ensure that the task is within the ability of the patients, regardless of background and skills. It must be possible to monitor the quality of articulation and phonation despite the acoustic noise in the MRI room, and data collection procedures must be reliable to minimise the number of repetitions and the amount of useless data obtained. All this must be achieved in as short a time as possible to minimise cost and maintain patient interest in the project.

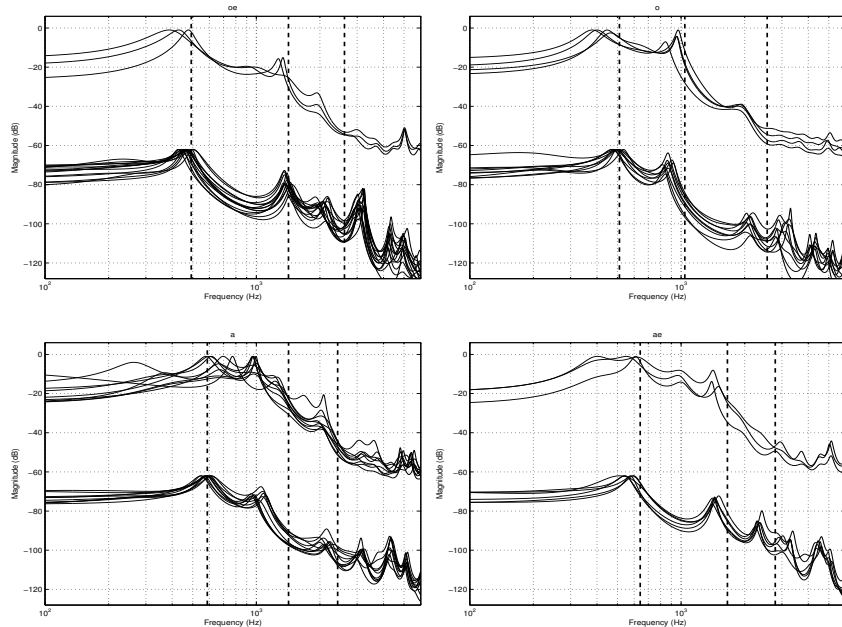


Figure 7: Spaghetti plots of LPC envelopes of Finnish back vowels [œ, o, a, æ]. The presentation is similar with Fig. 6.

The experimental setting and phonetic tasks require the patients to have abilities in concentration, remaining still, and sustaining prolonged phonation not significantly reduced from young adults in good health. At the time of writing of this article, seven patients (out of which four are female) have already undergone such MRI examinations preceding their orthognatic procedures, and they are expected to take part in a similar examination after their post-operative treatment will have been completed. All of these examinations have succeeded without any kind of complications, and the resulting MRI image and the speech sound data quality is very satisfactory as well. Applications to other patient groups are under consideration but may require adaptations to the required time of phonation and the total number of measurements.

Some questions and problems in the measurement arrangements remain open, in particular, involving acoustic noise and its impact on articulation. Acoustic noise during measurements remains a problem from two points of view. Firstly, formant extraction from de-noised, prolonged vowel samples is sometimes problematic as observed in Section 4.2. On the other hand, reliable formant extraction may be difficult for reasons unrelated with noise contamination: consider, e.g., vowels with low  $F_1$  in high pitch speech samples such as [i] pronounced by female subjects. Secondly, the onset of MRI noise may cause a significant adaptation in the patients' articulation. It may be possible to reduce this problem by running the 3D MRI sequence once while the patient receives the task instructions to adapt the patient to the noise, and a second time during phonation to obtain the vocal tract geometry. For the 2D sequences, the sequence may be started before phonation for the same effect.

## 6 Acknowledgements

The authors were supported by the Finnish Academy grant Lastu 135005, the Finnish Academy projects 128204 and 125940, European Union grant Simple4All, Aalto Starting Grant, Magnus Ehrnrooth Foundation, Åbo Akademi Institute of Mathematics, and Research Grant of Turku University Hospital.

The authors wish to thank professor P. Alku, Department of Signal Processing and Acoustics, Aalto University, for providing resources and consultation for the acquisition of comparison data in Figs. 6–7.

The current version of the post-processing software described in this article can be obtained from the authors by request. The raw MRI data, the speech sound data, and the surface models related to Figs. 6–7 are freely available for non-commercial academic and educational use.

## References

- [1] A. Aalto. A low-order glottis model with nonturbulent flow and mechanically coupled acoustic load. Master’s thesis, Aalto University, Department of Mathematics and Systems Analysis, 2009.
- [2] A. Aalto, D. Aalto, J. Malinen, and M. Vainio. Modal locking between vocal fold and vocal tract oscillations. arXiv:1211.4788 (submitted), 2013.
- [3] A. Aalto, P. Alku, and J. Malinen. A LF-pulse from a simple glottal flow model. In *Proceedings of the 6th International Workshop on Models and Analysis of Vocal Emissions for Biomedical Applications (MAVEBA2009)*, pages 199–202, 2009.
- [4] D. Aalto, O. Aaltonen, R.-P. Happonen, J. Malinen, P. Palo, R. Parkkola, J. Saunavaara, and M. Vainio. Recording speech sound and articulation in MRI. In *Proceedings of BIODEVICES 2011*, pages 168–173, 2011.
- [5] D. Aalto, J. Helle, A. Huhtala, A. Kivelä, J. Malinen, J. Saunavaara, and T. Ronkka. Algorithmic surface extraction from MRI data: modelling the human vocal tract. In *Proceedings of BIODEVICES 2013*, 2013.
- [6] D. Aalto, A. Huhtala, A. Kivelä, J. Malinen, P. Palo, J. Saunavaara, and M. Vainio. How far are vowel formants from computed vocal tract resonances? arXiv:1208.5963, 2012.
- [7] D. Aalto, J. Malinen, M. Vainio, J. Saunavaara, and J. Palo. Estimates for the measurement and articulatory error in MRI data from sustained vowel phonation. In *Proceedings of the International Congress of Phonetic Sciences*, 2011.
- [8] S. Boll. Suppression of acoustic noise in speech using spectral subtraction. *Acoustics, Speech and Signal Processing, IEEE Transactions on*, 27(2):113 – 120, 1979.
- [9] T. Chiba and M. Kajiyama. *The Vowel, Its Nature and Structure*. Phonetic Society of Japan, 1958.

- [10] K. Dedouch, J. Horáček, T. Vampola, and L. Černý. Finite element modelling of a male vocal tract with consideration of cleft palate. In *Forum Acusticum*, 2002.
- [11] H. K. Dunn. The calculation of vowel resonances, and an electrical vocal tract. *J. Acoust. Soc. Am.*, 22:740 – 753, 1950.
- [12] S. El Masri, X. Pelorson, P. Saguet, and P. Badin. Development of the transmission line matrix method in acoustics. applications to higher modes in the vocal tract and other complex ducts. *Int. J. of Numerical Modelling*, 11:133 – 151, 1998.
- [13] C. Ericsson. *Articulatory-Acoustic Relationships in Swedish Vowel Sounds*. PhD thesis, Stockholm University, Stockholm, Sweden, 2005.
- [14] G. Fant. *Acoustic Theory of Speech Production*. Mouton, the Hague, 1960.
- [15] A. Hannukainen, T. Lukkari, J. Malinen, and P. Palo. Vowel formants from the wave equation. *Journal of the Acoustical Society of America Express Letters*, 122(1):EL1–EL7, 2007.
- [16] H. L. F. Helmholtz. *Die Lehre von den Tonempfindungen als physiologische Grundlage für die Theorie der Musik*. Braunschweig: F. Vieweg, 1863.
- [17] J. Horáček, V. Uruba, V. Radolf, J. Veselý, and V. Bula. Airflow visualization in a model of human glottis near the self-oscillating vocal folds model. *Applied and Computational Mechanics*, 5:21–28, 2011.
- [18] R. Humphrey. <http://www.playrec.co.uk/>. Accessed Jul. 15th, 2012.
- [19] J.L. Kelly and C.C. Lochbaum. Speech synthesis. In *Proceedings of the 4th International Congress on Acoustics*, Paper G42: 1–4, 1962.
- [20] C. Lu, T. Nakai, and H. Suzuki. Finite element simulation of sound transmission in vocal tract. *J. Acoust. Soc. Jpn. (E)*, 92:2577 – 2585, 1993.
- [21] T. Lukkari, J. Malinen, and P. Palo. Recording speech during magnetic resonance imaging. In *Proceedings of the 5th International Workshop on Models and Analysis of Vocal Emissions for Biomedical Applications (MAVEBA2007)*, pages 163–166, 2007.
- [22] J. Makhoul. Linear prediction: A tutorial review. *Proceedings of the IEEE*, 63(4):561–580, 1975.
- [23] J. Makhoul. Spectral linear prediction: Properties and applications. *IEEE Transactions on Acoustics, Speech and Signal Processing*, 23(3):283 – 296, 1975.
- [24] J. Malinen and P. Palo. Recording speech during MRI: Part II. In *Proceedings of the 6th International Workshop on Models and Analysis of Vocal Emissions for Biomedical Applications (MAVEBA2009)*, pages 211–214, 2009.

- [25] J. Mullen, D. Howard, and D. Murphy. Waveguide physical modeling of vocal tract acoustics: Flexible formant bandwidth control from increased model dimensionality. *IEEE Transactions on Audio, Speech and Language Processing*, 14(3):964 – 971, 2006.
- [26] M. Niemi, J.P. Laaksonen, T. Peltomaki, J. Kurimo, O. Aaltonen, and RP Happonen. Acoustic comparison of vowel sounds produced before and after orthognathic surgery for mandibular advancement. *Journal of Oral & Maxillofacial Surgery*, 64(6):910–916, 2006.
- [27] H. Nishimoto, M. Akagi, T. Kitamura, and N. Suzuki. Estimation of transfer function of vocal tract extracted from MRI data by FEM. In *The 18th International Congress on Acoustics*, volume II, pages 1473–1476, 2004.
- [28] Optoacoustics, Ltd. <http://www.optoacoustics.com/>, 2009. Accessed Aug. 25th, 2009.
- [29] J. Palo, D. Aalto, O. Aaltonen, R.-P. Happonen, J. Malinen, J. Saunavaara, and M. Vainio. Articulating Finnish vowels: Results from MRI and sound data. *Linguistica Uralica*, 48(3):194–199, 2012.
- [30] P. Palo. *A wave equation model for vowels: Measurements for validation*. Licentiate thesis, Aalto University, Institute of Mathematics, 2011.
- [31] Praat v.4.6.15. <http://www.fon.hum.uva.nl/praat/>. Accessed July. 5th, (2010).
- [32] J. Přibíl, J. Horáček, and P. Horák. Two methods of mechanical noise reduction of recorded speech during phonation in an MRI device. *Measurement science review*, 11(3), 2011.
- [33] J. Přibíl, A. Přibilová, and I. Frollo. Analysis of spectral properties of acoustic noise produced during magnetic resonance imaging. *Applied Acoustics*, 73(8):687–697, 2012.
- [34] N. Rofsky, V. Lee, G. Laub, M. Pollack, G. Krinsky, D. Thomasson, M. Ambrosino, and J. Weinreb. Abdominal MR imaging with a volumetric interpolated breath-hold examination. *Radiology*, 212(3):876 – 884, 1999.
- [35] H. Suzuki, T. Nakai, N. Takahashi, and A. Ishida. Simulation of vocal tract with three-dimensional finite element method. *Tech. Rep. IEICE*, EA93-8:17 – 24, 1993.
- [36] K. Vahatalo, J.P. Laaksonen, H. Tamminen, O. Aaltonen, and RP Happonen. Effects of genioglossal muscle advancement on speech: an acoustic study of vowel sounds. *Otolaryngology - Head & Neck Surgery*, 132(4):636–640, 2005.
- [37] M. Vainio, A. Suni, H. Järveläinen, J. Järvikivi, and V. Mattila. Developing a speech intelligibility test based on measuring speech reception thresholds in noise for English and Finnish. *J. Acoust. Soc. Am.*, 118:1742–1750, 2005.
- [38] P. Šidlof, J. Horáček, and V. Řídký. Parallel CFD simulation of flow in a 3D model of vibrating human vocal folds. *Computers and Fluids*, 2012.

- [39] P. Švancara and J. Horáček. Numerical modelling of effect of tonsillectomy on production of Czech vowels. *Acta Acustica united with Acustica*, 92:681 – 688, 2006.
- [40] P. Švancara, J. Horáček, and L. Pešek. Numerical modelling of production of Czech vowel /a/ based on FE model of the vocal tract. In *Proceedings of International Conference on Voice Physiology and Biomechanics*, 2004.